Int. J. Heat Mass Transfer. Vol. 36, No. 10, pp. 2511–2526, 1993
Printed in Great Britain

0017-9310/93 $6.00+0.00

CHF mechanism in flow boiling from a short heated wall—I. Examination of near-wall conditions with the aid of photomicrography and high-speed video imaging

J. E. GALLOWAY† and I. MUDAWAR‡

Boiling and Two-Phase Flow Laboratory, School of Mechanical Engineering, Purdue University, West Lafayette, IN 47907, U.S.A.

(*Received* 11 *May* 1992 *and in final form* 1 *December* 1992)

Abstract—Results of flow visualization experiments are presented to clearly identify the trigger mechanism for critical heat flux (CHF) in flow boiling. It is shown that discrete bubbles which form following the onset of nucleation coalesce into a wavy vapor layer at fluxes well below CHF. Depressions in the layer interface were observed to touch the heater surface periodically, painting a thin liquid sub-film on the surface beneath the vapor layer. This sub-film was consumed by a combination of vigorous boiling and interfacial evaporation. As CHF was approached, boiling became more concentrated toward the leading edge of the heater surface and around regions where the vapor layer interface touched the surface, while the remaining parts of the surface were dry. CHF was exceeded when severe vapor effusion from the sub-film normal to the heater surface lifted the wavy interface away from the surface, precluding any sustained wetting and resulting in a global dry-out.

1. INTRODUCTION

EXTENSIVE research efforts have been focused on modeling the relevant physical processes leading to CHF. However, due to the difficulty in performing detailed flow visualization of the near-wall region at heat fluxes approaching CHF, many of the published CHF models have been based on postulated mechanisms and not verified through direct observation.

Several flow visualization studies have been performed in pursuit of identifying the CHF mechanism and determining the conditions leading to CHF during flow boiling. Gunther [1] observed a dramatic increase in vapor volume in the form of large vapor clusters ('clumps') that enveloped the heater surface as CHF approached, particularly on the surface downstream locations. At heat fluxes just below CHF, Fiori and Bergles [2] observed intense boiling in a liquid sub-film trapped beneath similar vapor clusters. Using an electrical probe, they estimated the sub-film thickness to be at least 0.06 mm. Tong and Hewitt [3] and Cumo *et al.* [4] suggested coalescence into large vapor volumes is caused by larger bubbles penetrating further away from the viscous wall region, which enables these bubbles to travel faster than, and overtake smaller bubbles.

The increase in bubble coalescence prior to CHF was reported in many studies involving flow boiling in narrow annuli. Van der Molen and Galijee [5] noted narrow annular spacings gave rise to large clusters of vapor at CHF whereas in larger annular spacings, CHF occurred when a thick bubble boundary layer formed near the heater surface. Several layers of bubbles were distributed normal to the heater surface at downstream locations, while some bubbles coalesced into larger vapor slugs. Tolubinskiy *et al.* [6] reported that CHF was not affected by channel spacing for spacings larger than 1.3 mm. Hung and Yao [7] reported a reduction in CHF for annular channel spacings less than 0.80 mm. CHF in very narrow channels resulted from evaporation of a thin liquid sub-film trapped beneath 'squeezed' bubbles.

Using a microthermocouple probe, Hino and Ueda [8, 9] recorded temperature fluctuation within the bubble layer close to a heated surface to determine bubble frequency and the vapor residence period near the surface. They observed that, as the heat flux was increased close to CHF, the bubble frequency decreased sharply and the ratio of vapor residence period to the liquid residence period increased remarkably especially at downstream locations, evidenced by longer periods of high temperature fluctuation. These observations point to the disappearance of the discrete bubble regime and the initiation of a fairly continuous vapor layer at heat fluxes below CHF.

Tong and Hewitt [3] and Mattson *et al.* [10] noted a

†Present address: Cummins Engine Company, Columbus, IN 47202, U.S.A.

‡Author to whom all correspondence should be addressed.

NOMENCLATURE

$c_{p,f}$	specific heat of liquid	ΔT_{sub}	liquid subcooling upstream of heater, $T_{sat}-T_m$.
h_{fg}	latent heat of vaporization		
q	heat flux	Greek symbols	
T_m	liquid temperature upstream of heater	ν_f	kinematic viscosity of liquid
T_s	heater surface temperature	ν_g	kinematic viscosity of vapor
T_{sat}	saturation temperature	ρ_f	liquid density
U_m	mean liquid velocity upstream of heater	ρ_g	vapor density
ΔT_{sat}	heater surface superheat, T_s-T_{sat}	σ	surface tension.

reduction in bubble coalescence near the heater surface with increasing pressure. Mattson *et al.* also reported larger bubbles formed by coalescence were torn away from the heater surface as the core velocity increased, but these bubbles did not affect CHF since they were concentrated away from the heater surface and were too few in number. Instead, CHF was caused by coalescence of the smaller bubbles close to the heater surface into thin vapor blankets.

Transient boiling heat transfer was observed to be a dominant mechanism prior to reaching CHF, particularly at low pressures. Many investigators reported measuring dry periods, as noted by a rise in surface temperature, followed by rewetting periods accompanied by a sudden drop in surface temperature. Increasing the thermal capacitance of the heater delayed CHF from occurring during the periods of intermittent dry-out. Fiori and Bergles [2] measured a 58% increase in CHF when the heater wall thickness was increased from 0.305 mm to 1.98 mm. Del Valle [11] developed an empirical CHF correlation accounting for the effects of subcooling and heater wall thickness for thicknesses ranging between 0.08 and 0.20 mm. Up to a 57% increase in CHF was measured for the thickest wall. However, his empirically-based correlation suggests CHF would not increase with increasing wall thickness for thicknesses greater than 0.5 mm. The influence of wall thickness was more pronounced at high liquid subcoolings.

It is generally accepted that bubble coalescence in one form or another is a precursor to CHF. Van der Molen and Galijee [5], Anderson and Minns [12] and Hino and Ueda [8, 9] all postulated that CHF occurs when the dry-out period between successive liquid slugs becomes long enough for the surface temperature to rise above the Leidenfrost temperature, thereby preventing liquid rewetting of the heater surface. However, it is not clear from these studies whether exceeding the Leidenfrost temperature is a result of, or the actual cause of CHF.

It is evident from the above review that several interdependent processes contribute to the initiation of CHF in flow boiling systems. They include (1) bubble coalescence into large vapor clusters or blankets at high fluxes, (2) sharp increase in the residence period of vapor clusters, and (3) dryout of a liquid sub-film (sublayer) beneath the vapor clusters. However, it is not clear which of these processes constitutes the *trigger* mechanism for CHF. The primary objective of the present study is to identify this mechanism by relying on detailed photomicrographic and videographic analysis of near-wall conditions at heat fluxes up to and exceeding CHF.

2. EXPERIMENTAL METHODS

An experimental apparatus was constructed to facilitate detailed photomicrographic analysis of liquid–vapor exchange and interfacial features near the heater surface as CHF was approached and exceeded. The experimental apparatus consisted of a flow channel, flow loop and photographic hardware. An overview of the photographic methods and equipment will be presented first, followed by a description of the flow channel and flow loop.

2.1. *Photographic methods*

Obtaining photographs of flow boiling was complicated by the small sizes of bubbles and other interfacial features, often smaller than 1 mm, and large flow velocities, exceeding 2 m s^{-1} for some of the conditions studied. Large magnifications were required which reduced the depth of field, causing blurring of the liquid–vapor interface due to lateral interfacial displacement along the viewing axis. In addition, high-speed photography demanded intense lighting to capture and freeze the motion of the liquid–vapor interface.

The flow channel was designed with a narrow flow gap and small heater width, capturing the equivalent of a narrow slice of the boiling flow normal to the viewing axis. This configuration reduced lateral motion of bubbles normal to the plane of view while keeping the depth of field manageable. Optical access was available through two transparent windows, enabling photographs to be taken with back lighting, thereby reducing lighting requirements and clearly isolating the liquid–vapor interface as a silhouette.

An NAC model E10 16 mm high-speed film-based camera, capable of up to 10 000 frames per second,

was used with the high velocity tests. Unfortunately, clear reproduction and enlargement of the 16 mm film was not possible for the desired film segments; however, the flow details were clearly visible when projected on a screen. A Kodak Ektapro 1000 video motion analyzer, capable of up to 6000 partial frames per second, was used for flow velocities smaller than $2\ m\ s^{-1}$. Clear video images were recorded at these low velocities using an Infinity model CFM microscope. A 3500 watt incandescent light source with a frosted glass diffuser was used for back lighting. Heating by the light source was minimized by illuminating the flow channel in short intervals and also by covering the flow channel with a reflecting foil. Video imaging at rates of 3000 frames per second or greater required the full light source intensity to clearly illuminate the flow.

Still photographs were taken with a Nikon FM2 35 mm still camera with a Questar model QM1 long range microscopic lens system at magnifications up to $\times 60$. A Vivitar model 283 flash, modified with a high speed flash accessory, produced a 1/30 000 s flash duration that clearly illuminated the flow and froze interfacial motion. A thin sheet of mylar was placed between the flash and flow channel to diffuse the light burst. A General Radio stroboscope light source was utilized during the focusing of the camera lens before taking each photograph. The camera shutter was set to a slow speed, 1/250 s, and the laboratory lights were turned off. Afterwards, the camera was triggered, which first opened the shutter and then activated the high-speed flash, exposing the film for a short duration.

2.2. *Flow visualization channel*

Figure 1 shows a cross-sectional view of the flow visualization module. The flow passage was constructed by milling a 0.16×0.64 cm slot into a thick Lexan plate. A second Lexan plate served as a cover for the flow channel. A leak proof seal was maintained by an o-ring fitted between the two plates. The heater, with a 0.16×1.27 cm boiling surface area, was inserted flush with the channel wall and sealed to the Lexan channel with an o-ring mounted at the heater flange base. Two round quartz windows sandwiched the heater in place, exposing a clear unobstructed view of the boiling surface. Scaling of high magnification photographs was referenced to a 0.35 mm hole drilled just to the side of the flow channel in the same viewing plane as the heater. The heater length, 1.27 cm, was used as a reference scale for low magnification photographs.

Figure 2 shows a planar view of the flow channel. The fluid entered the module at a right angle to the flow channel. A honeycomb flow straightener, with a ten-to-one length-to-diameter ratio, was placed upstream from the channel inlet to remove swirl from the inlet flow. An entry length 120 times the channel hydraulic diameter provided fully developed hydrodynamic conditions before reaching the heater. All tests were conducted in an up-flow configuration with the heater surface oriented parallel to the gravity vector to preclude any body force normal to the heater surface.

Pressure and temperature sensors monitored the flow conditions upstream and downstream from the heater. At each of the two locations, measurements from a thermocouple and a pressure transducer were used to determine the thermodynamic state of the fluid. The upstream pressure was measured by a Sensotec 0–6.9 bar pressure transducer calibrated to an accuracy of 0.07 bar. A Sensotec 0–1.0 bar differential pressure transducer measured the pressure drop across the heater with an accuracy better than

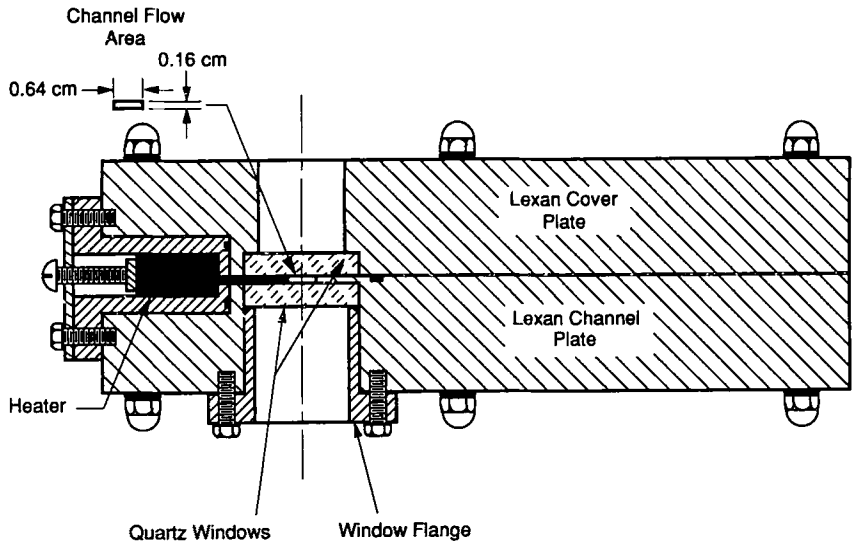

FIG. 1. Cross-sectional view of flow visualization channel (section A-A in Fig. 2).

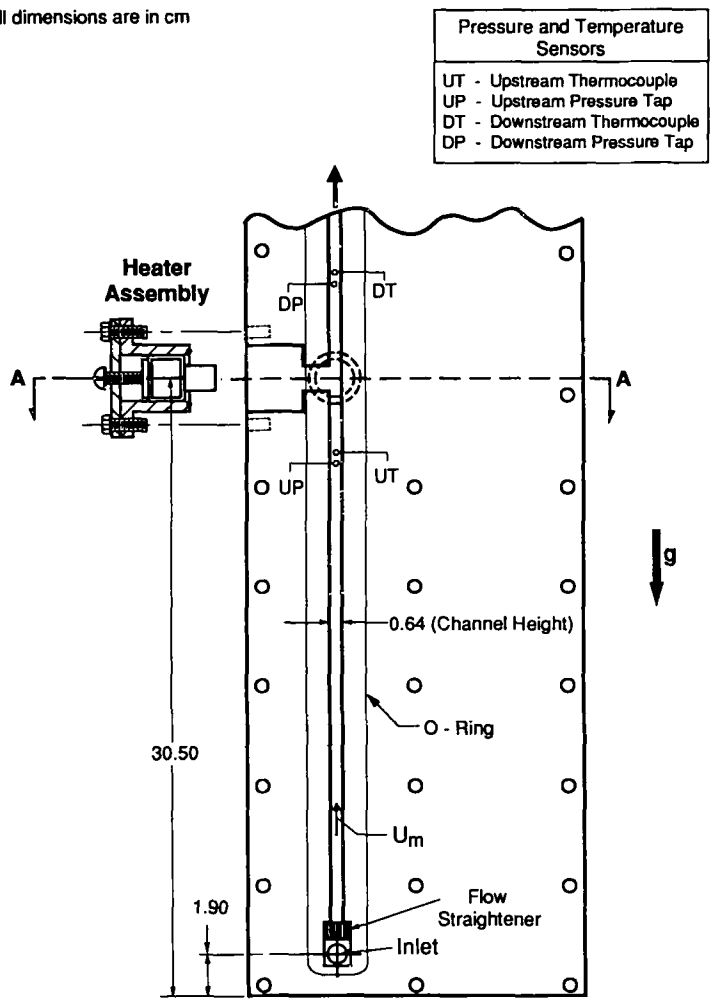

FIG. 2. Planar view of the flow channel plate (with the cover removed) and heater assembly.

0.001 bar. Type-K thermocouples, having a diameter of 0.076 mm, were used to measure the bulk flow temperatures. They were mounted 2.5 mm downstream from the pressure taps to avoid influencing the pressure measurements.

The heater was constructed by silver-soldering a thick-film resistor to the backside of the oxygen-free copper block as shown in Fig. 3. Five type-K thermocouples having a diameter of 0.076 mm were mounted along the centerline of the heater at 0.25 cm intervals from the boiling surface. The thermocouples were calibrated by placing the heater module in an oven and measuring all five temperatures once steady-state thermal conditions were achieved. The calibration was repeated for several steady-state conditions ranging from room temperature to 100°C, the temperature expected at CHF for the fluid tested. During calibration, none of the five thermocouples deviated from the average value by more than 0.1°C.

The heater power was supplied from a 120 V a.c. variac. To avoid the uncertainties associated with correcting electrical power measurements, both the heat flux at the boiling surface and the surface temperature were determined indirectly using a second-order polynomial fitted to steady-state temperatures read from the five thermocouples mounted along the heater centerline. Maximum uncertainties in the calculated heat flux and surface temperature as a result of errors in the thermocouple measurement and the thermocouple positioning are estimated to be 8% and ± 0.2°C, respectively.

2.3. *Flow loop*

Figure 4 shows a schematic diagram of the flow loop and accessories used to maintain the desired channel inlet conditions. FC-87, a 3M dielectric fluid, was chosen because of its relatively low boiling temperature (30°C at 1.0 atm) which reduced the possibility of overheating the flow visualization module or destroying the heater after repeated CHF tests. The thermophysical properties of FC-87 at the operating pressure of the present study, 1.37 bar, are given in Table 1. Liquid FC-87 was pumped from the reservoir and metered by a bypass valve to the desired flow rate.

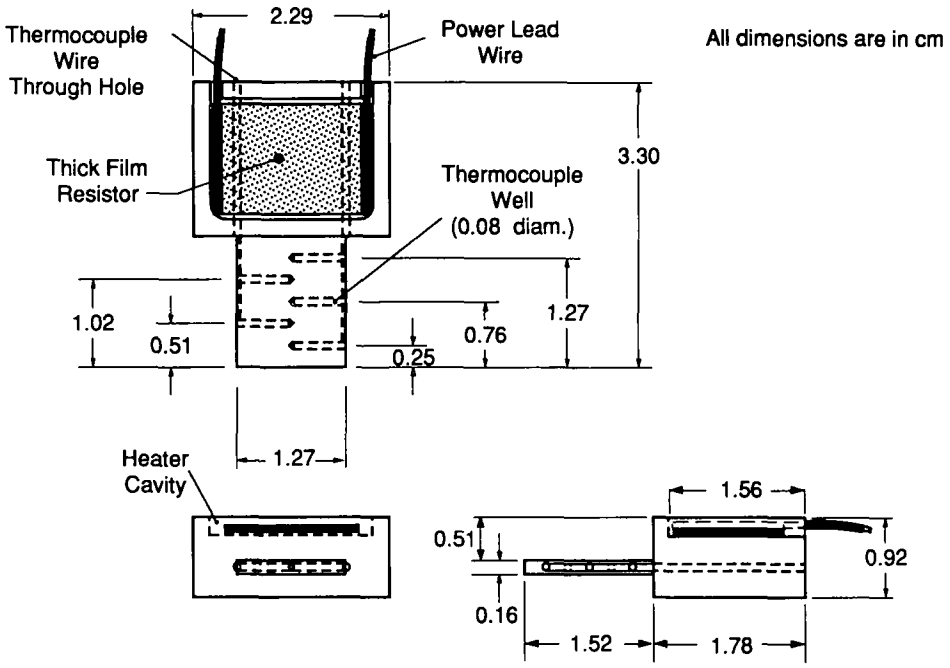

FIG. 3. Heater construction.

A rotameter was calibrated to measure inlet velocities in the range from 0.35 to 2.25 m s^{-1} with an accuracy better than $\pm 3\%$. The liquid inlet temperature was controlled by adjusting electrical power input to an in-line electrical heater or water flow rate through a heat exchanger located downstream from the pump and fine tuned with the aid of the in-line heater. The upstream pressure, measured at the flow channel upstream pressure tap, was regulated by adjusting the electrical power input to the immersion heaters in a dearation tank. A dearation procedure was conducted to remove any air entrained in the flow loop by boiling liquid FC-87 from the dearation tank and condensing the vapor in a reflux condenser. An 8°C subcooling at 1.37 bar was maintained upstream from the heater during all tests in order to examine boiling at near saturated conditions without the danger of flashing liquid FC-87 as it passed over the heater surface.

3. FLOW VISUALIZATION

Photographs were taken over the full range of heat fluxes leading to CHF. High magnification photographs were taken to examine the shapes of detached bubbles while full heater photographs traced the bubble coalescence as CHF was approached and exceeded.

Table 1. Properties of saturated FC-87 and 1.37 bar (T_{sat} = 39°C)

$c_{p,f}$	1099 J kg^{-1} K^{-1}
h_{fg}	85 500 J kg^{-1}
σ	10.9×10^{-3} N m^{-1}
ν_f	2.57×10^{-7} m^2 s^{-1}
ν_g	7.15×10^{-7} m^2 s^{-1}
ρ_f	1742 kg m^{-3}
ρ_g	16.8 kg m^{-3}

3.1. *Discrete bubble regime*

Figure 5 shows bubbles nucleating at the middle of the heater surface at heat fluxes slightly above the onset of nucleate boiling. Discrete bubbles were observed to grow and detach from the heater surface and occasionally coalesce to form larger bubbles further downstream. At low velocities, $U_m = 0.35$ m s^{-1}, detached bubbles were spherical and traveled at least 0.10 mm above the heater surface. As the flow velocity increased, the bubbles became more oblong, stretching in the stream-wise direction three to four times the bubble diameter. A distinct liquid sub-film was observed to be trapped between the discrete elongated bubbles and the heater surface, having a thickness less than 0.06 mm for the bubble shown in the photograph corresponding to $U_m = 1.5$ m s^{-1}.

3.2. *Coalescent bubble regime*

Full heater length photographs were taken at increasing heat fluxes as shown in Fig. 6 with corresponding identification numbers marked on the boiling curves given in Fig. 7. The discrete bubbles depicted in Fig. 5 formed at the onset of nucleate boiling and traveled over the heater surface with a distinct separation distance. At heat fluxes above 40% of CHF, discrete bubbles generated at upstream nucleation sites merged downstream to form larger coalescent bubbles having small separation distances.

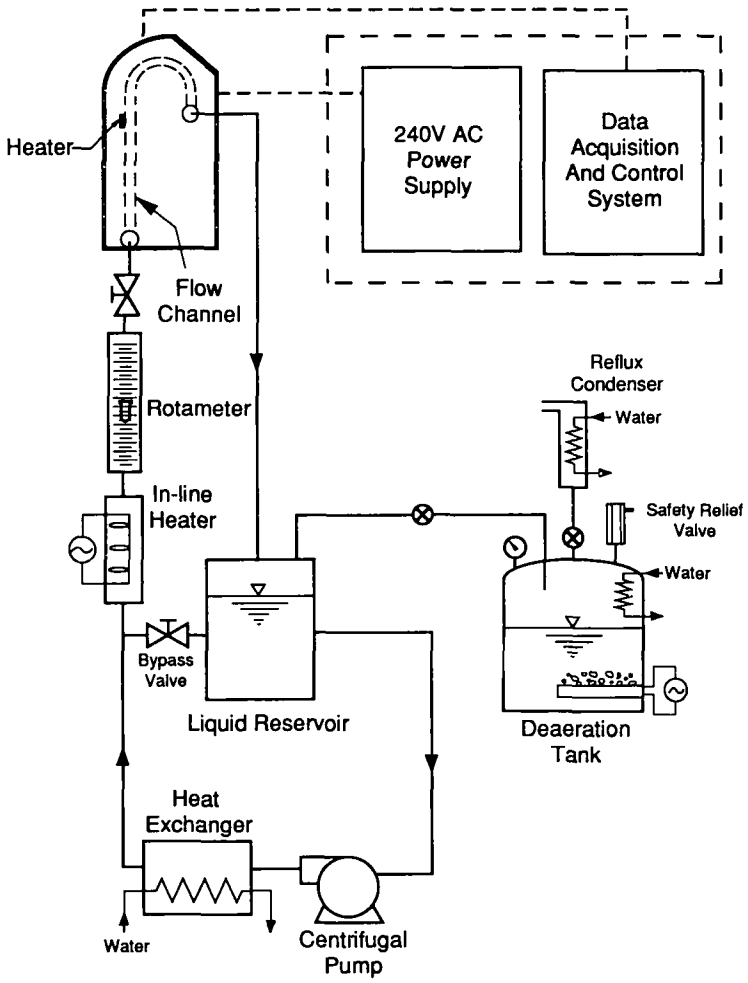

FIG. 4. Schematic diagram of flow loop.

3.3. *Wavy liquid–vapor layer regime*

Above 60% of CHF, discrete bubbles disappeared entirely on the trailing edge of the heater and were replaced by a continuous wavy vapor layer that periodically touched the heater surface as shown in Fig. 6 for $U_m = 0.5$ m s^{-1}, picture 3. Additional increases in heat flux moved the point at which bubbles first coalesced into a vapor layer further upstream. Occasionally, for heat fluxes above 85% of CHF, a continuous vapor layer covered the entire heater surface. It was quickly replaced by discrete bubbles on the heater upstream surface while the wavy vapor layer remained on the trailing edge. Additional increases in heat flux promoted a more continuous vapor coverage of the heater surface.

Liquid was intermittently supplied to the surface through the vapor layer when the interface made contact with the heater at locations of maximum displacement in the wavy liquid–vapor interface. These locations, hereafter called wetting fronts, appeared to spread a thin liquid sub-film over the entire surface. Vapor was ejected into the vapor layer by a violent burst of minute discrete bubbles within the sub-film and evaporation of the sub-film interface, contrary to the vapor jet model postulated by Haramura and Katto [13].

At stable heat fluxes approximately equal to 95% of CHF, known hereafter as CHF (−), portions of the heater surface became dry before the passage of the next wetting front. Liquid contact with the heater surface became exceedingly difficult as CHF approached, as noted by a reduction in the slope of the boiling curve shown in Fig. 7, signalling a transition to a less efficient mode of boiling within discrete wetting fronts rather than over the entire surface.

3.4. *Critical heat flux*

The highest heat flux that gave a stable surface temperature was recorded as CHF. Boiling at CHF was observed to occur primarily at the leading edge and underneath the wetting fronts. At heat fluxes slightly greater than CHF, but less than a few seconds after the temperature excursion commenced, known hereafter as CHF (+), boiling was observed only at the leading edge of the heater and within the wetting fronts. Once CHF had been exceeded, wetting fronts

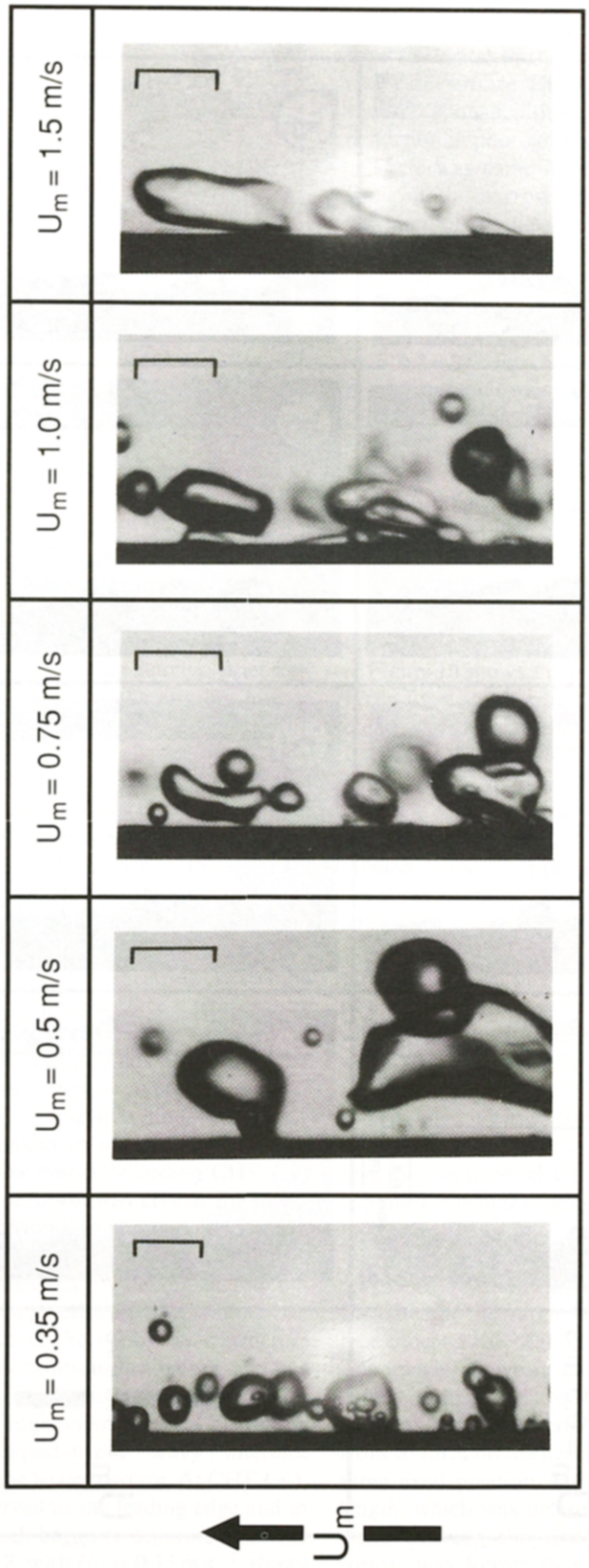

FIG. 5. Photographs of discrete bubbles at the middle of the heater surface. Each photograph was taken at the indicated magnification.

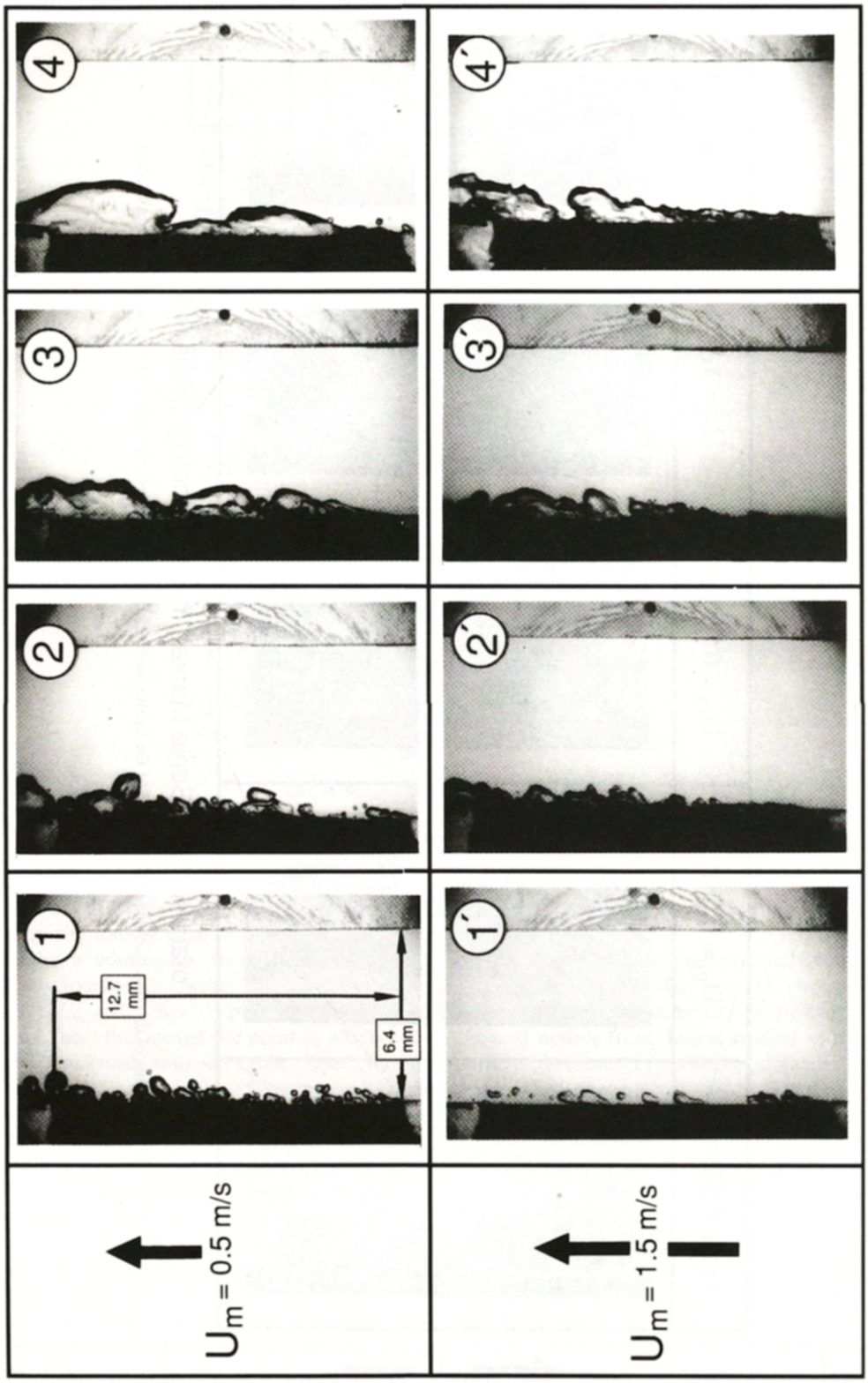

FIG. 6. Full heater length photographs at increasing heat fluxes. The identification numbers shown correspond to the boiling curves given in Fig. 7.

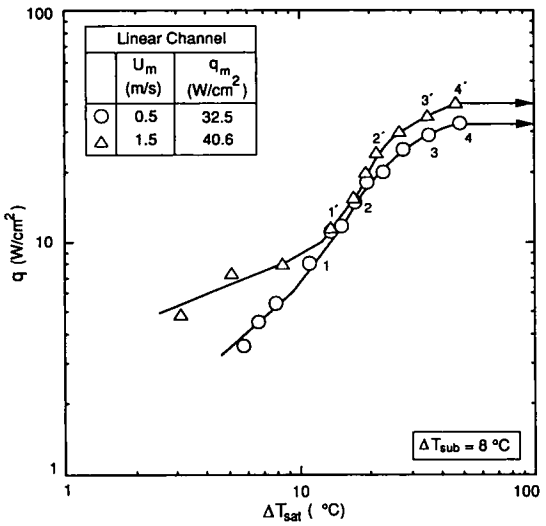

FIG. 7. Boiling curves at two different flow velocities.

began lifting away from the heater surface, giving the appearance of a continuous vapor blanket that covered the entire surface. The supply of liquid to the heater surface was restricted, extinguishing most of the remaining downstream boiling activity. Brief wetting did occur after CHF, but the ensuing intense boiling precluded any persistent liquid contact with the surface.

Additional photographs were taken at CHF (−) and CHF (+) to contrast changes in the vapor layer flow structure as CHF commenced. CHF (+) was initiated by an incremental increase in the electrical power to exceed the heat flux corresponding to the highest stable surface temperature. The surface temperature began to rise slowly starting from a stable value of approximately 85°C. After exceeding approximately 92°C, the surface temperature increased at a much faster rate and the electrical power to the heater was automatically cut off by the data acquisition and control system to avoid any damage to the heater and flow visualization module.

Extreme care was taken to maintain steady-state conditions in the heater before recording CHF (−) photographs. This precaution was crucial for identifying the *trigger* condition that initiated CHF. CHF (+) photographs were taken immediately after the surface temperature began to rise uncontrollably but a few seconds before the electrical power was cut off.

A distinct difference in the vapor layer structure was observed between conditions just before, and just after CHF as shown in Fig. 8. At CHF (−), the heater surface displayed vigorous boiling activity at wetting fronts where the liquid–vapor wavy interface remained attached to the heater surface. At CHF (+), boiling was only observed at the leading edge and in the wetting fronts which began to separate from the heater surface. Figure 8, with $U_m = 0.35\ \text{m s}^{-1}$, shows the first wetting front lifting from the heater surface. Wetting fronts were lifted more frequently as the CHF process progressed. CHF (+) photographs at flow velocities less than $1.25\ \text{m s}^{-1}$ clearly show dry regions between wetting fronts and wetting fronts being lifted from the heater by the action of vigorous boiling from the heater surface. Higher flow velocities show similar results although with less clarity because of the slight distortion in photography at these velocities.

There was some initial concern whether the side walls of the narrow flow channel might affect the waviness of the liquid–vapor interface and whether similar wave characteristics would prevail in wider channels. However, a similar behavior was observed by Willingham *et al.* [14], Fig. 9, in the flow boiling of FC-72 on a 1.0 cm square heater flush mounted in a 0.2×2.0 cm channel. Vapor was observed to propagate downstream from the leading edge in the form of a two-dimensional vapor wave.

3.5. *CHF trigger mechanism*

Chronological sequences of flow visualization photographs, taken of a high-pitch video screen using a Nikon FM2 35 mm camera, were used to identify and record the mechanism responsible for initiating CHF. Two sequences are discussed, showing the motion of wetting fronts at CHF (−) and CHF (+).

Figure 10 shows a chronological sequence of events taken for a stable condition at CHF (−) with a reference scale marked in mm shown in the background. Boiling at wetting fronts supplied vapor to the wavy vapor layer while portions of the heater surface between consecutive wetting fronts remained dry in the absence of liquid contact. Two wetting fronts, labeled 1 and 2, appeared on the heater surface at $t = 0$ ms corresponding to the first video sequence shown. At $t = 2$ ms, a depression in the liquid–vapor interface approached the heater surface which later established a wetting front, labeled +1, at $t = 6$ ms at a point further downstream. Finally, at $t = 10$ ms, another depression in the liquid–vapor interface approached the heater surface preparing to establish another wetting front. This sequence repeated itself, forming new wetting fronts at an upstream location which then propagated over the heater surface removing the supplied electrical energy until it passed beyond the heater trailing edge.

Wetting fronts appeared to be formed by a growth of instabilities in the liquid–vapor interface. When the amplitude of interfacial displacement approached the thickness of the vapor layer, the liquid–vapor interface touched the heater and created a wetting front. The images shown in Fig. 10 (and many others not shown in this paper) reveal that interfacial instability acted as a wave generator, forcing the first wetting front to form on the heater surface consistently at the same axial position. However, the measured wavelength, which was determined as the separation distance between the centers of consecutive wetting fronts, was longer than the distance between the heater leading edge and the center of the first wetting front. This observation suggests that after a wetting

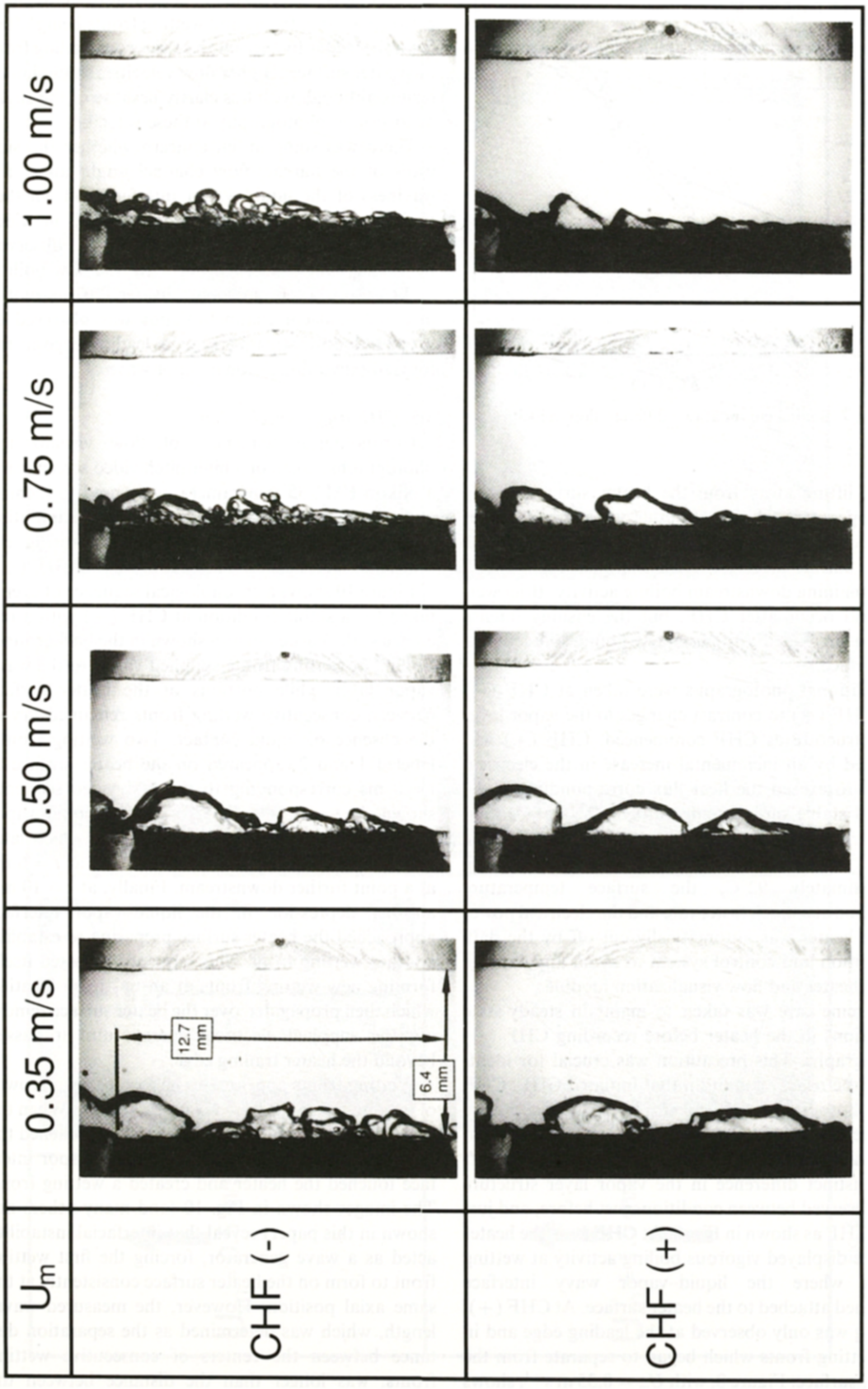

FIG. 8. CHF (−) and CHF (+) photographs at increasing velocities.

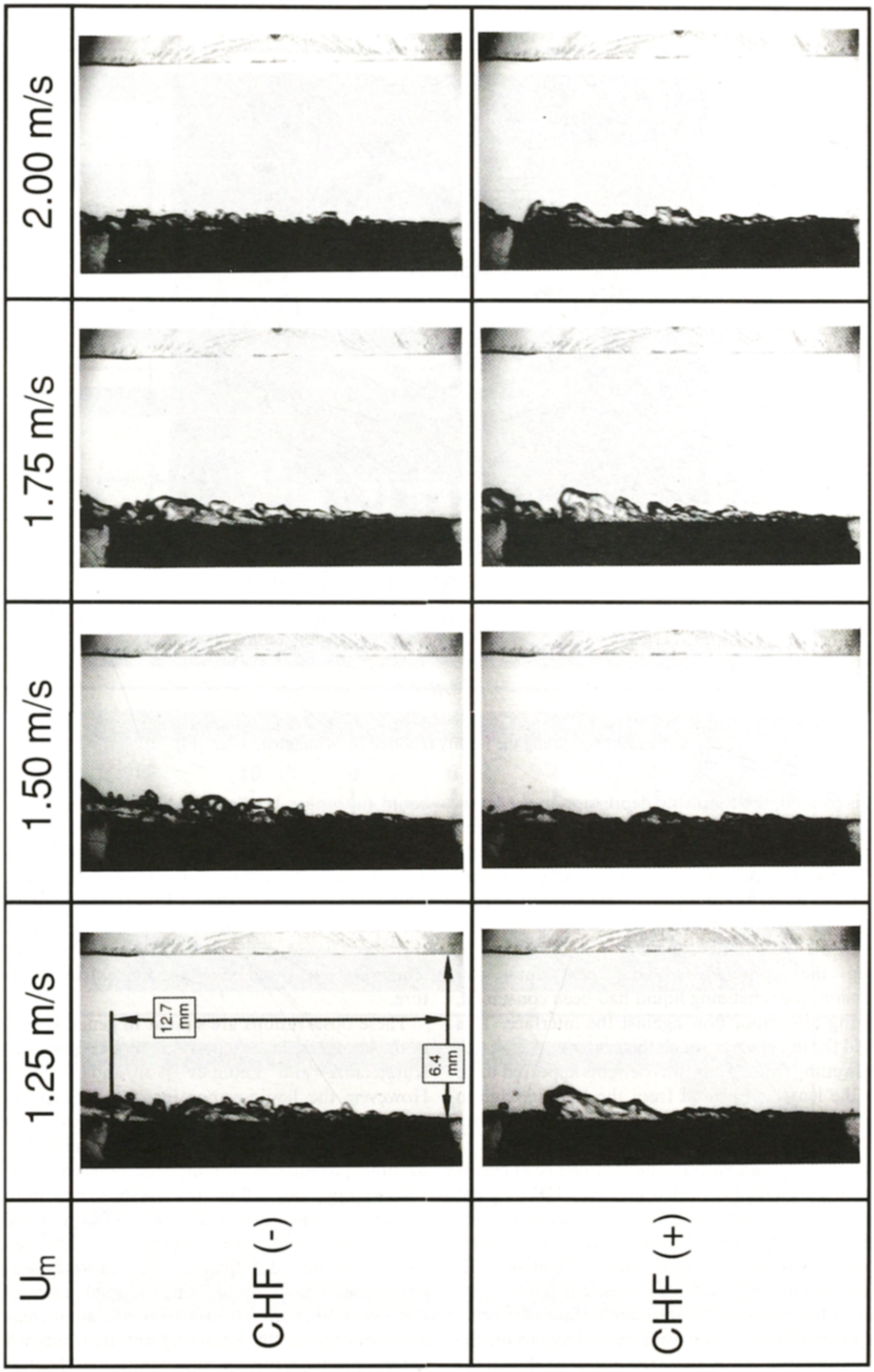

FIG. 8—*Continued.*

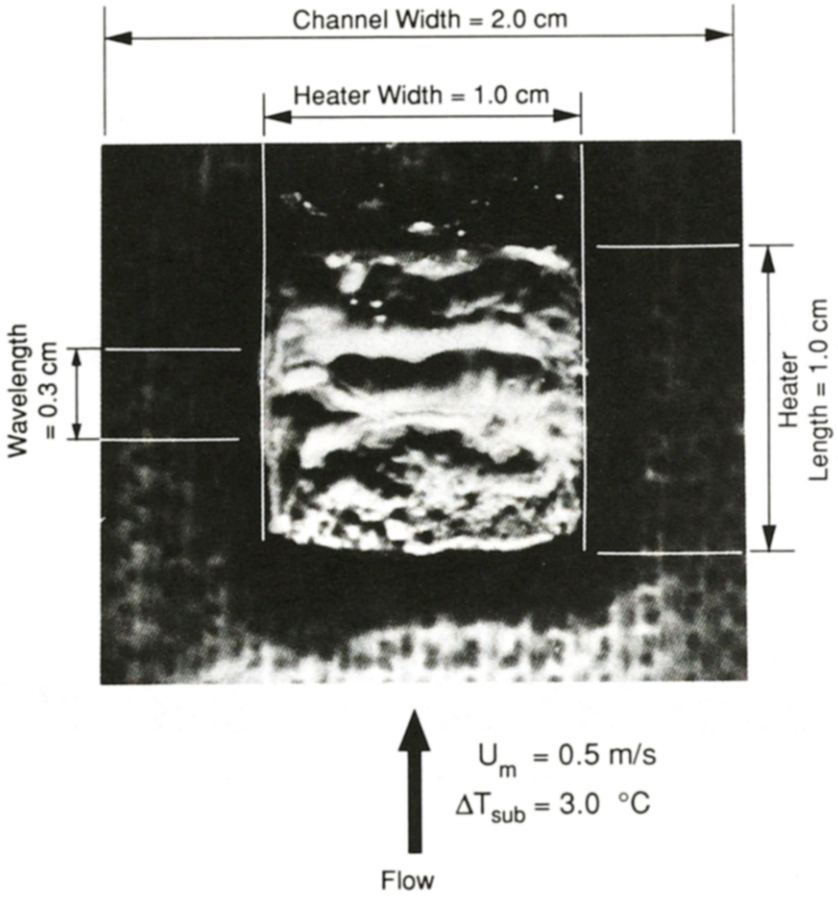

FIG. 9. Normal view of CHF in FC-72 boiling on a 1.0 cm square heater flush mounted in a 0.2 × 2.0 cm flow channel taken using the facility reported by Willingham *et al.* [14].

front is formed, the following depression in the interface fails to establish a new wetting front, thereby doubling the interfacial wavelength. Near the leading edge intense boiling activity and vapor effusion were observed to push the approaching interface away from the surface, delaying the formation of a wetting front until the arrival of a new depression in the interface. During the approach of the next interfacial depression, the remaining liquid had been consumed, removing any vapor flow against the interface. This allowed the interface to touch the heater and establish a new wetting front. Thus, wavelengths appeared to be twice the length measured from the leading edge to the point where the first wetting front made contact with the heater surface.

Figure 11 shows a chronological sequence of events recorded on high-speed video tape at CHF (+). At $t = 3$ ms, the first wetting front was lifted away, causing the liquid–vapor interface to flatten at the point of contact with the dry heater surface. Unlike CHF (−) conditions where wetting fronts remained in contact with the previously dry heater surface, the efflux of vapor at CHF (+) was sufficiently large to lift the first wetting front away from the heater as shown for times $t = 3$, 5 and 7 ms in Fig. 11. As a result of the decreased liquid contact, the supplied electrical power could no longer be dissipated by boiling. Thus, the heater surface temperature began to increase, promoting a drastic increase in localized boiling activity at the remaining wetting fronts. Therefore, despite the occasional interfacial contact with the heater surface, the ensuing intense vapor production precluded any sustained liquid contact even though the surface temperature was well below the Leidenfrost temperature.

These observations are similar in general outcome to the boundary layer separation models proposed by Kutateladze and Leont'ev [15] and Tong [16]. However, the liquid–vapor interface trigger mechanism reported here resulted from the localized boiling activity at wetting fronts and not from the hydrodynamic conditions forcing the separation of a dispersed two-phase flow from the heater surface.

Figure 11 illustrates a *cascading* effect initiated by a small increase in power resulting in the first wetting front becoming deactivated. This process is *catastrophic* and not gradual since a small increase in electrical power input leads to a significant increase in local heat flux in the remaining wetting fronts which, in turn, produces further concentration of the thermal energy and deactivation of wetting fronts. Wetting becomes less available during departure to film

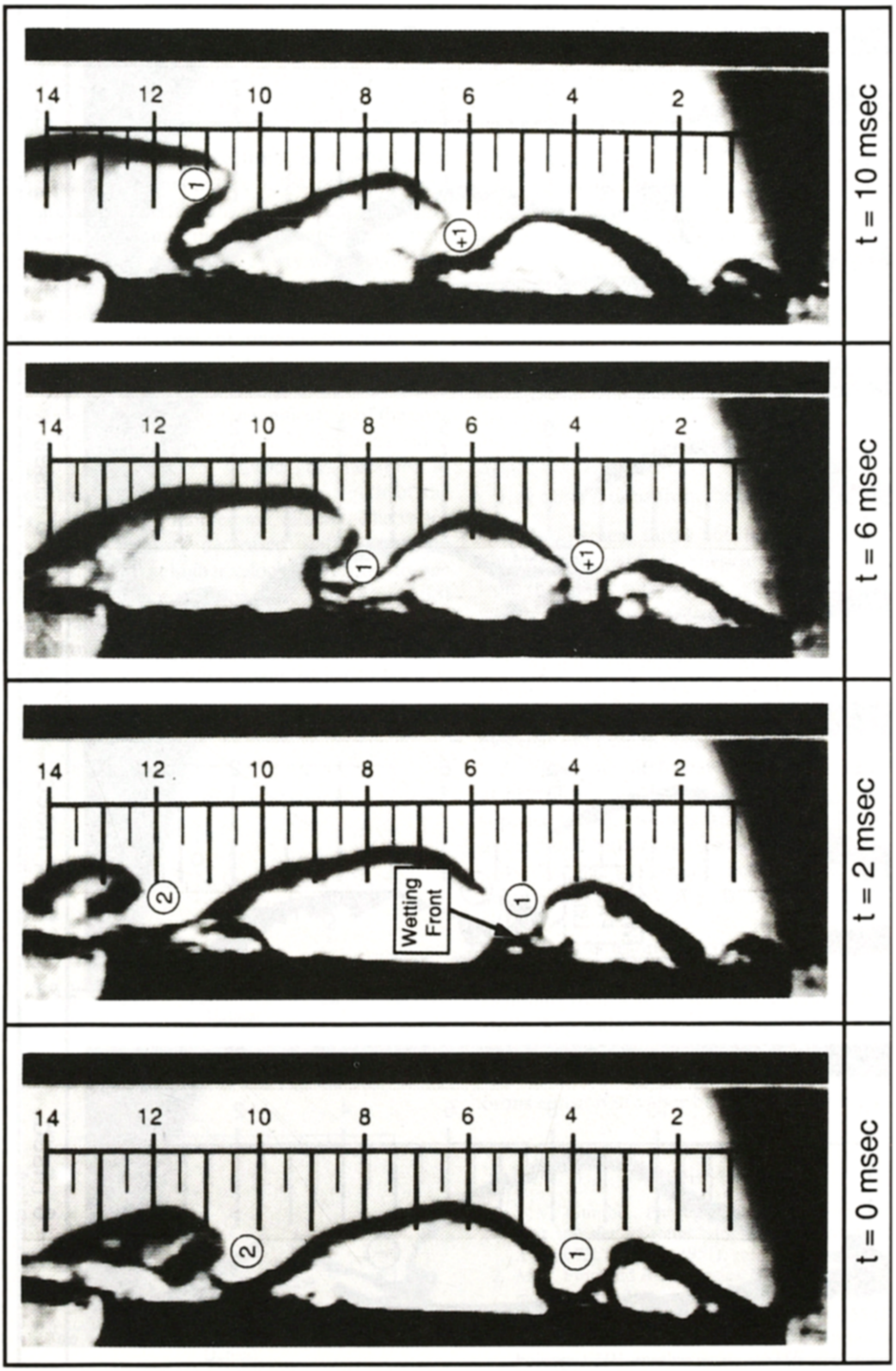

FIG. 10. Chronological sequence of events showing propagation of wetting fronts at CHF (—) for $U_m = 0.35\ m\ s^{-1}$.

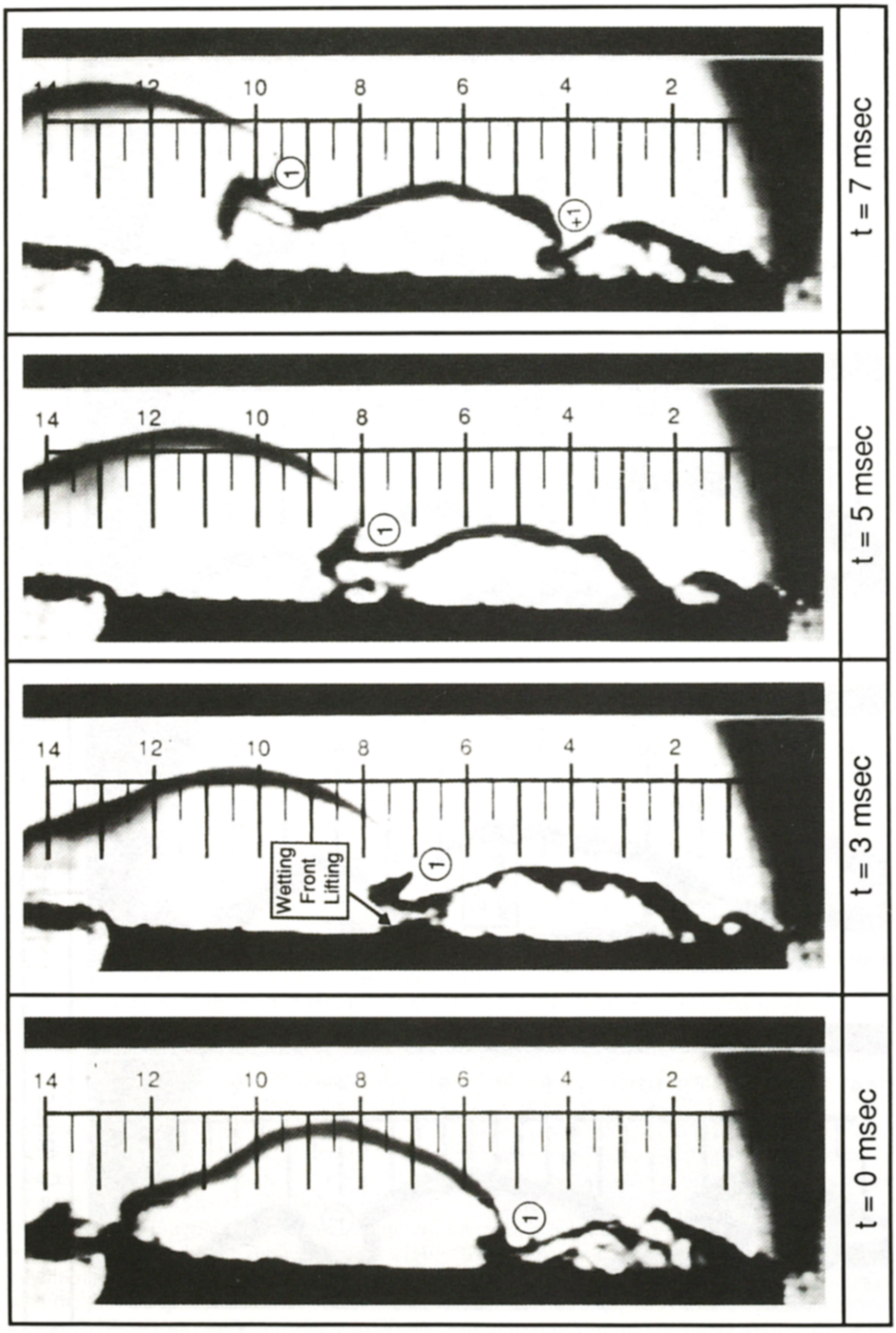

FIG. 11. Chronological sequence of events showing lifting of wetting fronts at CHF (+) for $U_m = 0.35\ m\ s^{-1}$.

boiling. The rate of this departure is obviously dependent upon the thermal mass of the heater.

3.6. *Vapor wave features at CHF*

Measurements from the individual high-speed video frames were used to determine the vapor layer amplitude and wavelength at CHF (−). The wavelength was measured as the stream-wise distance between two wetting fronts and the vapor layer amplitude as the normal distance from the heater to the wave peak. The random nature of the interfacial waviness necessitated performing statistical averaging of observations randomly picked over an elapsed time interval of approximately 1 s. Thirty wavelength and vapor layer amplitude measurements, taken at each velocity tested, were averaged and the results are shown in Figs. 12(a) and (b), respectively, with error bars indicating one standard deviation about the mean. A measurement accuracy of 0.1 mm was attained using the combined magnification of the continuous focus microscope and a 55 cm wide video monitor. The vapor layer wavelength, measured at a downstream location two-thirds the length of the heater, decreased with increasing velocity. The vapor layer amplitude also decreased with increasing velocity, especially at higher velocities. A three-to-one wave aspect ratio (i.e. wavelength to amplitude ratio) remained approximately constant over the entire range of flow velocities tested. These results prove the flow field has a strong influence on the hydrodynamic instability of the liquid–vapor interface and the ensuing CHF.

Part 2 of this study [17] will incorporate the observations of interfacial contact with the heater surface with a hydrodynamic instability model to predict both the interfacial features (vapor layer thickness, wavelength, etc.) and the magnitude of CHF.

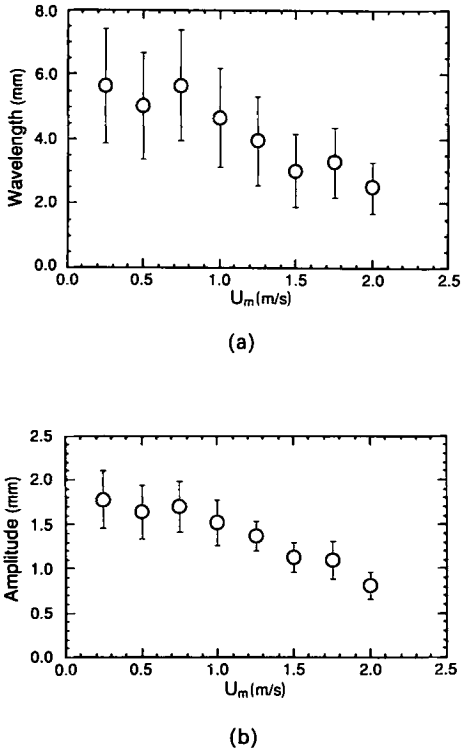

FIG. 12. Vapor wave measurements. (a) Vapor layer wavelength. (b) Vapor layer amplitude.

4. CONCLUSIONS

A new understanding has emerged for the CHF trigger mechanism based upon both microscopic and macroscopic observations of the near-wall region. CHF was approached when the heat flux reached a sufficiently high level to cause coalescence of vapor bubbles into a wavy vapor layer. Minimum points in the liquid–vapor interface periodically touched the heater surface, thereby wetting the heater locally while other locations remained dry. After exceeding CHF, the effusion of vapor normal to the heater surface lifted the wavy interface away from the heater causing surface dry-out.

Key observations from the study are as follows:

1. At low heat fluxes and low velocities, discrete bubbles appeared hemispherical and departed normal from the heater surface. At higher velocities, bubbles were elongated in the stream-wise direction and slid over the heater surface.
2. At low heat fluxes and high velocities, a liquid sub-film, having a thickness less than 0.06 mm, was observed to be trapped below discrete elongated bubbles that slid over the heater surface.
3. Vapor bubbles coalesce into large vapor waves at heat fluxes about 60% of CHF while liquid was supplied through wetting fronts when the depressions in the liquid–vapor interface touched the surface.
4. The heater surface between wetting fronts became increasingly dry as heat flux approached CHF.
5. Vapor effusion from the boiling surface into the vapor waves was not caused by minute vapor jets stemming from a liquid sub-film, but rather from violent boiling and evaporation from the liquid sub-film.
6. CHF was observed to commence after wetting fronts were lifted from the boiling surface by a vigorous effusion of vapor beneath the fronts.

REFERENCES

1. F. C. Gunther, Photographic study of surface-boiling heat transfer to water with forced convection, *Trans. ASME* **73**, 115–123 (1951).
2. M. P. Fiori and A. E. Bergles, Model of critical heat flux in subcooled flow boiling, *Proc. 4th Int. Heat Transfer Conf.*, Versailles, France, Vol. 6, pp. 354–355 (1970).
3. L. S. Tong and G. F. Hewitt, Overall viewpoint of flow boiling CHF mechanisms, *ASME Paper 72-HT-54* (1972).
4. M. Cumo, G. E. Farello, G. Ferrari and M. Montannari, Boiling sublayers along heated walls, *A.I.Ch.E. Symp. Series* **73**, 14–20 (1977).

5. S. B. van der Molen and F. W. Galijee, The boiling mechanism during burnout phenomena in subcooled two-phase water flows, *Proc. 6th Int. Heat Transfer Conf.*, Toronto, Canada, Vol. 1, pp. 381–385 (1978).
6. V. I. Tolubinskiy, A. K. Litoshenko and V. L. Shevtsov, Correlation of experimental data on critical heat fluxes in annular channels, *Heat Transfer—Sov. Res.* **1**(1), 80–87 (1(969).
7. Y. H. Hung and S. C. Yao, Critical heat flux of convective Freon-113 in very narrow annuli, *ASME Paper 83-HT-10* (1983).
8. R. Hino and T. Ueda, Studies on heat transfer and flow characteristics in subcooled flow boiling—Part 1. Boiling characteristics, *Int. J. Multiphase Flow* **11**, 269–281 (1985).
9. R. Hino and T. Ueda, Studies on heat transfer and flow characteristics in subcooled flow boiling—Part 2. Flow characteristics, *Int. J. Multiphase Flow* **11**, 283–297 (1985).
10. R. J. Mattson, F. G. Hammitt and L. S. Tong, A photographic study of the subcooled flow boiling crisis in Freon-113, *ASME Paper 73-HT-39* (1973).
11. M. V. H. Del Valle, An experimental study of critical heat flux in subcooled flow boiling at low pressure including the effect of wall thickness, *Proc. ASME-JSME Thermal Engineering Joint Conf.*, Honolulu, Hawaii, Vol. 1, pp. 143–150 (1983).
12. G. H. Anderson and D. E. Minns, Nucleate boiling in a flowing liquid, *Proc. 4th Int. Heat Transfer Conf.*, Versailles, France, Vol. 4, pp. 1–11 (1970).
13. Y. Haramura and Y. Katto, A new hydrodynamic model of critical heat flux, applicable widely to both pool and forced convection boiling on submerged bodies in saturated liquids, *Int. J. Heat Mass Transfer* **26**, 389–399 (1983).
14. T. Willingham, C. Gersey and I. Mudawar, Forced-convection boiling from an array of in-line heat sources in a flow channel, *Proc. ASME/JSME Thermal Engineering Joint Conf.*, Reno, Nevada, Vol. 2, pp. 365–374 (1991).
15. S. S. Kutateladze and A. I. Leont'ev, Some applications of the asymptotic theory of the turbulent boundary layer, *Proc. 3rd Int. Heat Transfer Conf.*, Chicago, Illinois, Vol. 3, pp. 1–6 (1966).
16. L. S. Tong, Boundary-layer analysis of the flow boiling crisis, *Int. J. Heat Mass Transfer* **11**, 1208–1211 (1968).
17. J. E. Galloway and I. Mudawar, CHF mechanism in flow boiling from a short heated wall—II. Theoretical CHF model, *Int. J. Heat Mass Transfer* **36**, 2527–2540 (1993).